eLIFE elifesciences.org

RESEARCH ARTICLE

Figures and figure supplements

The molecular basis for an allosteric inhibition of K^+-flux gating in K_{2P} channels

Susanne Rinné *et al*

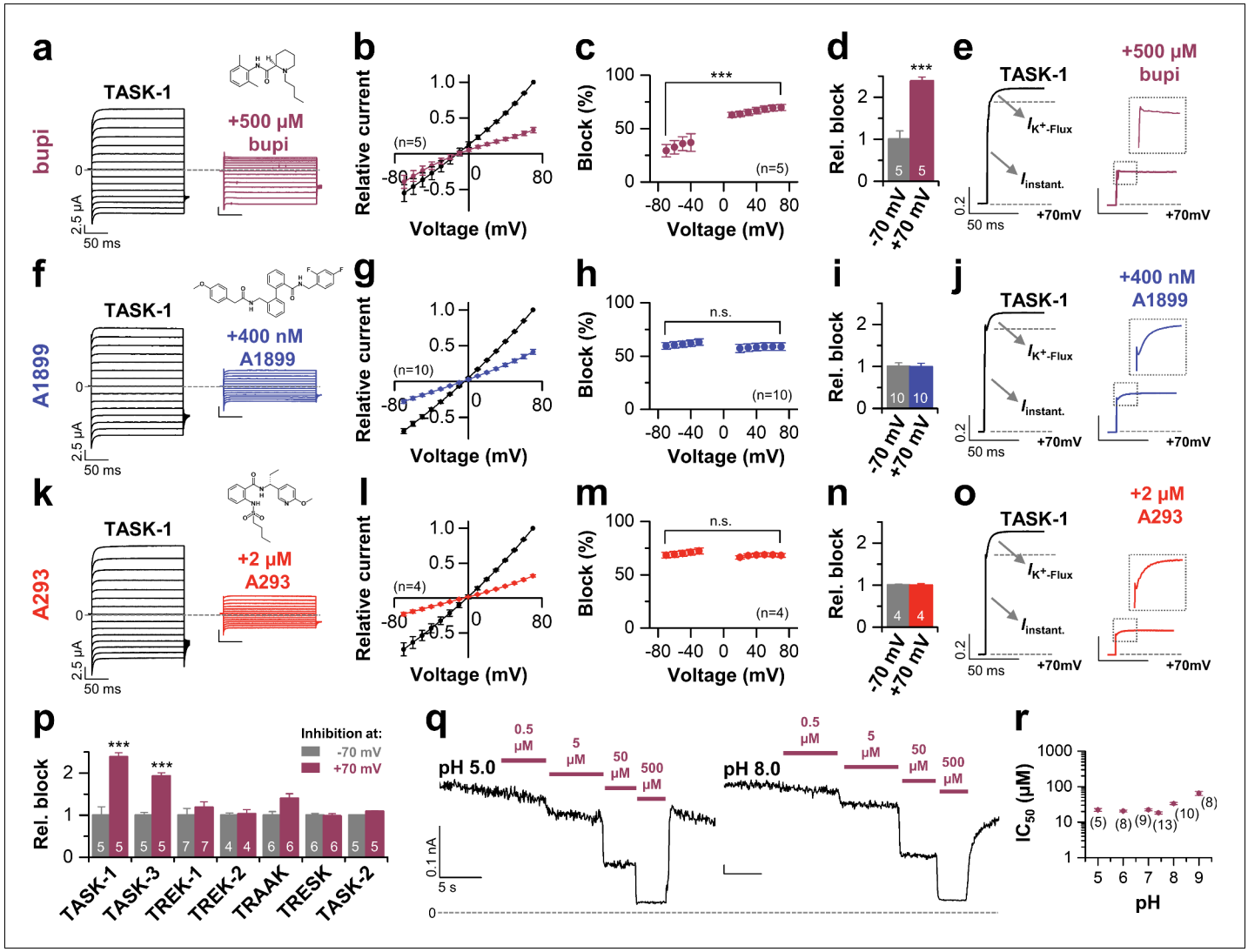

Figure 1. Voltage-dependent block of TASK-1 by impaired outward K^+-flux gating. (**a**) Representative current traces of TASK-1 injected oocytes before (black) and after (purple) application of 500 µM bupivacaine, recorded in a symmetrical potassium solution (KD96) at potentials ranging from −70 mV to +70 mV. (**b**) Average IV-relationships recorded before and after drug application. (**c**) Analyses of the inhibition by bupivacaine at different voltages. (**d**) Relative block by bupivacaine comparing the inhibition at −70 and +70 mV, recorded under symmetrical potassium concentrations. (**e**) Mean current kinetics before (left) and after (right) application of 500 µM bupivacaine, illustrating the instantaneous ($I_{instant}$) and K^+-flux gated ($I_{K^+\text{-flux}}$) current component of the TASK current. Note, the lack of a K^+-flux gated component after application of bupivacaine. (**f–j**) As in (**a–e**), but for A1899 or (**k–o**) for A293. (**p**) Relative block by bupivacaine comparing the inhibition of different K_{2P} channels at −70 mV and +70 mV, recorded under symmetrical potassium concentrations. (**q**) Representative measurements of TASK-3 channels from inside-out macropatches showing the inhibition by increasing concentrations of bupivacaine at pH 5.0 (left) and pH 8.0 (right), recorded at a constant potential of +60 mV. (**r**) IC_{50} values of TASK-3 inhibition by bupivacaine at various intracellular pH levels. Data are represented as mean ± S.E.M.. The numbers of experiments (n) are indicated within brackets or as small insets in the respective bars.

DOI: https://doi.org/10.7554/eLife.39476.002

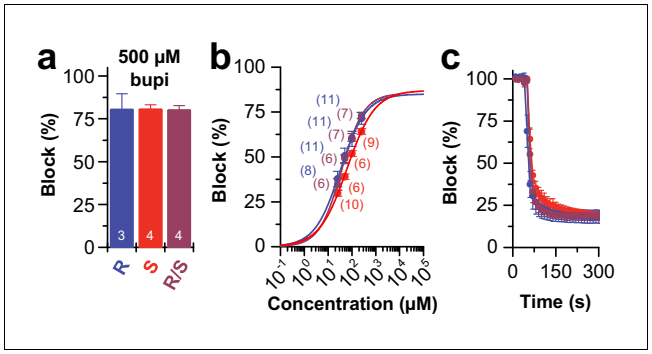

Figure 1—figure supplement 1. Block of TASK-1 channels by different bupivacaine enantiomers. (**a**) Inhibition of TASK-1 by bupivacaine R/S (purple), bupivacaine R (blue) and bupivacaine S (red) analyzed at +40 mV and (**b**) the respective dose-response curves. (**c**) Wash-in and onset of TASK-1 inhibition by 500 µM of the two enantiomers or the racemic drug (n = 4–9). Data are presented as mean ± S.E.M.. The numbers of experiments (n) are indicated within the respective bars or in brackets.

DOI: https://doi.org/10.7554/eLife.39476.003

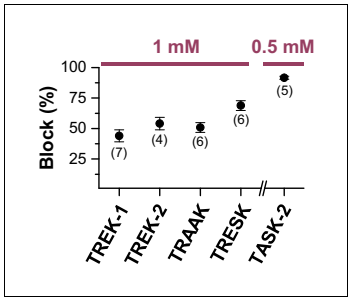

Figure 1—figure supplement 2. Block of different K_{2P} channels by bupivacaine. Percentage of block for different K_{2P} channels by 1 or 0.5 mM bupivacaine recorded at +70 mV in KD96 solution. Data are presented as mean ± S.E.M.. The numbers of experiments (n) are indicated within the respective brackets.

DOI: https://doi.org/10.7554/eLife.39476.004

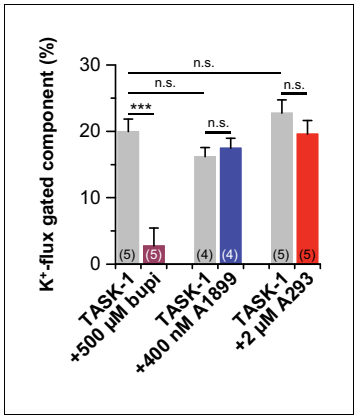

Figure 1—figure supplement 3. Block of K^+-flux gating by bupivacaine. K^+-flux gated components of the currents at +70 mV were analyzed before and after drug application. Note that only significant change to K^+-flux gated component of the currents happens after bupivacaine application. Data are presented as mean ± S.E.M.. The numbers of experiments (n) are indicated within the respective brackets. n.s. stands for 'not significant', ***, indicates $p < 0.001$ using a paired Student's t-test.

DOI: https://doi.org/10.7554/eLife.39476.005

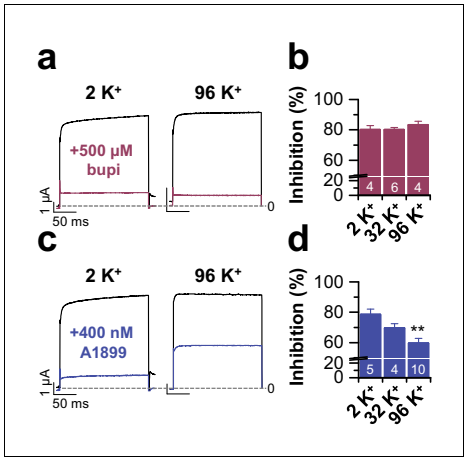

Figure 1—figure supplement 4. TASK-1 block by bupivacaine does not depend on the extracellular potassium concentration. (**a**) Block of TASK-1 by 500 µM bupivacaine is not altered by increased external potassium concentration. Representative current traces from voltage steps to +40 mV and (**b**) the analysis of block at different extracellular potassium concentrations (2 to 96 mM). (**c**) Inhibition of TASK-1 by 400 nM of the open channel blocker A1899 depends on the extracellular potassium concentration, as previously described (***Streit et al., 2011***). Representative currents recorded from voltage steps to +40 mV and (**d**) the analysis of block at different extracellular potassium concentrations (2 to 96 mM). Here gradually increasing the extracellular potassium concentration decreased TASK-1 inhibition by A1899. Data are presented as mean ± S.E.M.. The numbers of experiments (n) are indicated within the respective bars. **, indicates $p < 0.01$ using an unpaired Student's t-test.

DOI: https://doi.org/10.7554/eLife.39476.006

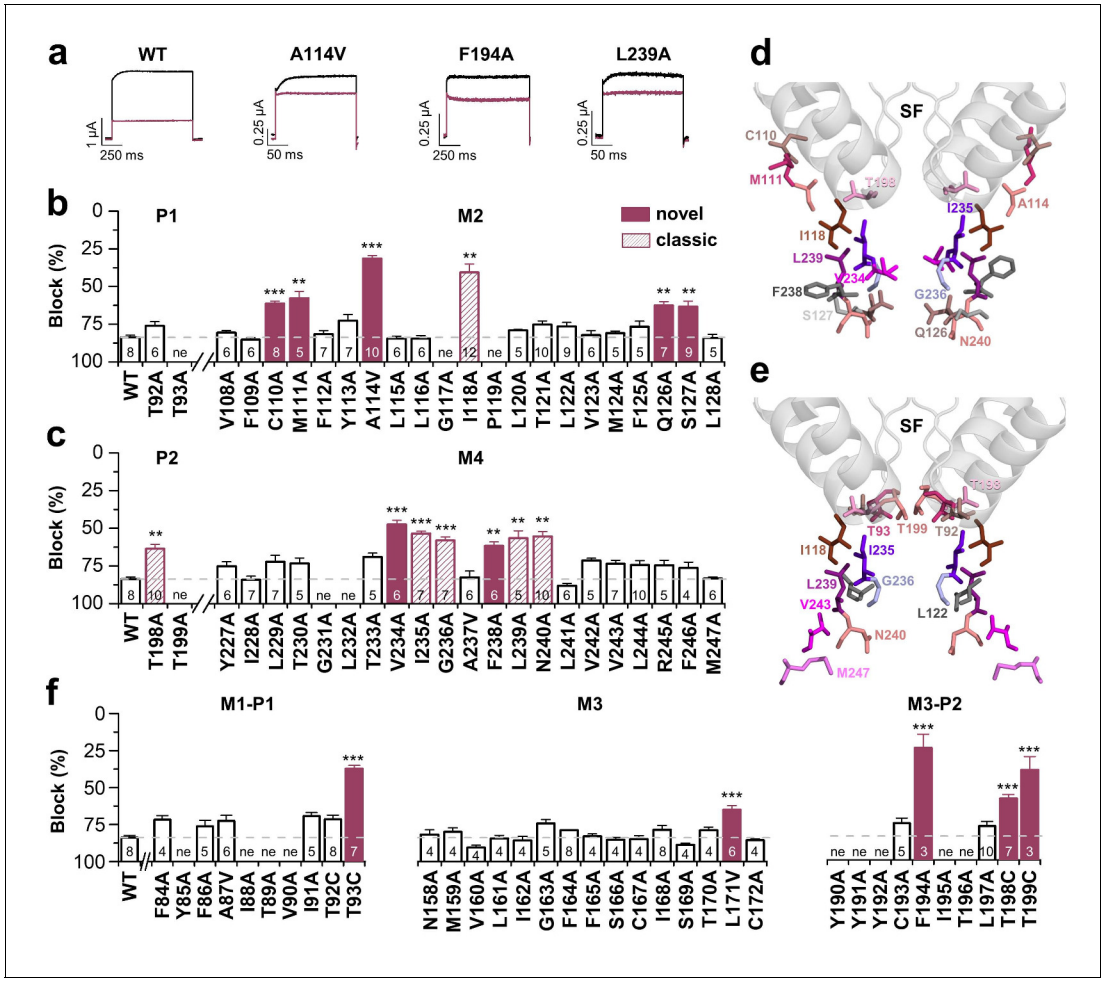

Figure 2. Bupivacaine utilizes a novel binding site in TASK-1. (**a**) Representative current traces of wild-type TASK-1 (WT) and mutant channels expressed in oocytes before (black) and after (purple) application of 500 µM bupivacaine. (**b**) Percentage of inhibition by 500 µM bupivacaine of wild-type TASK-1 and alanine mutants of the P1 signature sequence, the M2 segment and (**c**) the P2 signature sequence and the M4 segment. Residues identified as drug-binding sites ('hits'), which were previously also reported for the binding site of the open channel blocker A1899 ('classical'), are illustrated as striated bars and the 'hits' of the novel bupivacaine binding site are depicted as filled bars ('novel'). (**d**) Amino acids involved in binding of bupivacaine and (**e**) the respective A1899 binding mode, according to ***Ramírez et al. (2017)***, both illustrated in a TRAAK-OO (PDB ID: 3UM7) based TASK-1 homology model. SF indicates the selectivity filter. (**f**) Analyses of the percentage of inhibition by 500 µM bupivacaine for TASK-1 alanine mutants of the M1-P1, M3 and M3-P2 segments. ne, not expressed. Data are represented as mean ± S.E.M.. The numbers of experiments (**n**) are indicated within the respective bars.

DOI: https://doi.org/10.7554/eLife.39476.007

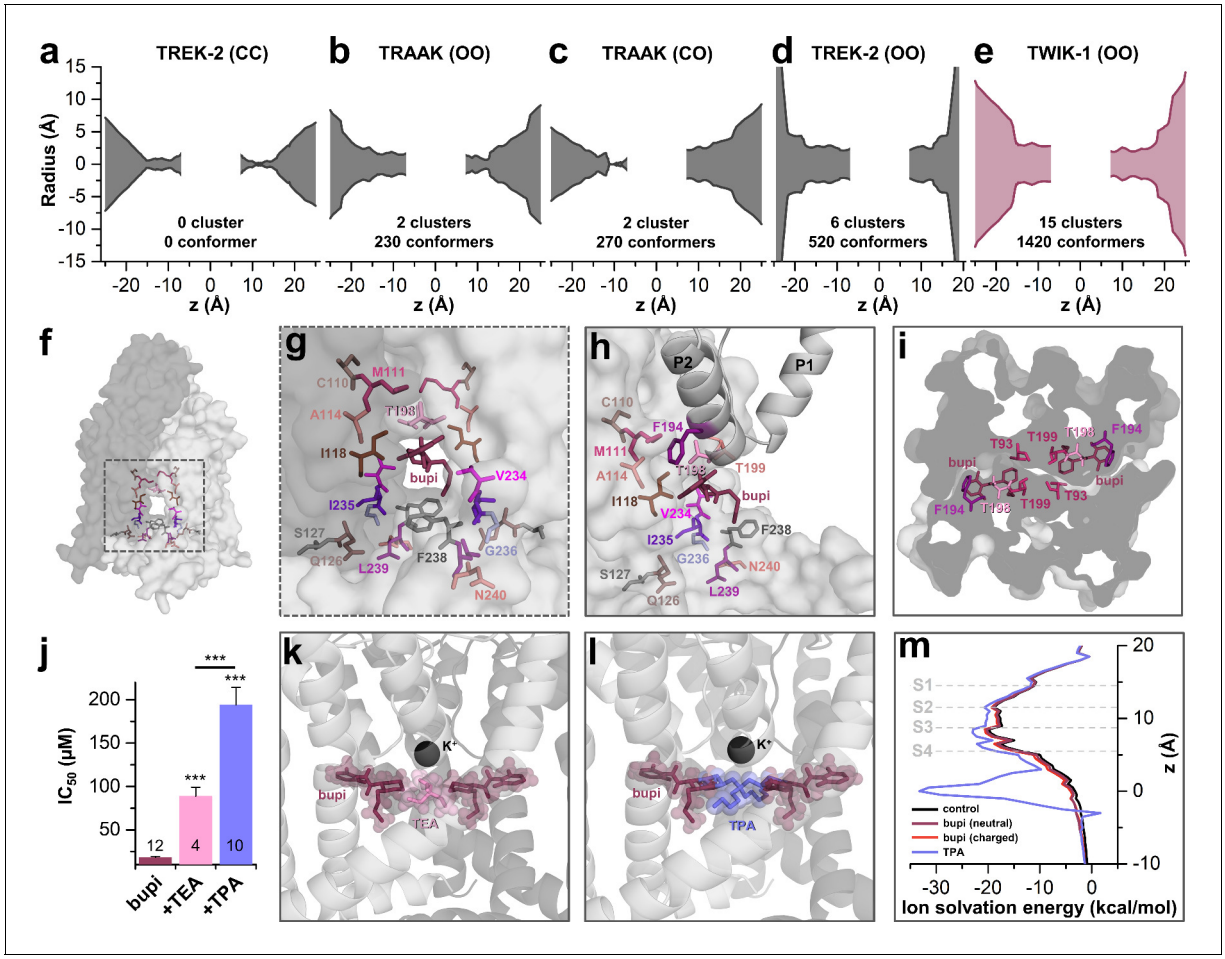

Figure 3. TASK-1 channels are fenestrated providing the bupivacaine binding site. (**a–e**) Hole analyses illustrating the diameter of the side fenestrations in different TASK-1 homology models together with the number of docking solutions (conformers) located in the fenestrations and the number of significant clusters formed by the different conformers. 'C' indicates a closed and 'O' an open fenestration. The TASK-1 homology models were based (**a**) on TREK-2-CC (PDB ID: 4BW5), (**b**) TRAAK-OO (PDB ID: 3UM7), (**c**) TRAAK-CO (PDB ID: 4I9W), (**d**) TREK-2-OO (PDB ID: 4XDK), and (**e**) TWIK-1-OO (PDB ID: 3UMK). (**f**) TASK-1 homology model based on TWIK-1 illustrating the amino acid 'hits' in the M2 and M4 segments identified by alanine scanning. Note that the 'hits' primarily line the side fenestrations. (**g**) Enlargement of (**f**) with bupivacaine located in the side fenestrations illustrating the involvement of the M2 and M4 hits. (**h**) View showing the localization of bupivacaine under the second pore helix together with the respective M2 and M4 'hits'. (**i**) Cross section view from the bottom of the TASK-1 model visualizing the two side fenestrations and the localization of bupivacaine together with the 'hit' residues of the pore helices. (**j**) IC_{50} of bupivacaine on TASK-3 channels recorded in inside-out macropatch clamp experiments alone or in the presence of TEA or TPA. (**k**) Binding mode of bupivacaine together with that of TEA and (**l**) TPA, respectively. (**m**) Ion solvation free energy profile for potassium ions in the TWIK-1 based TASK-1 pore homology model alone (control), in the presence of neutral or charged bupivacaine or TPA.
DOI: https://doi.org/10.7554/eLife.39476.008

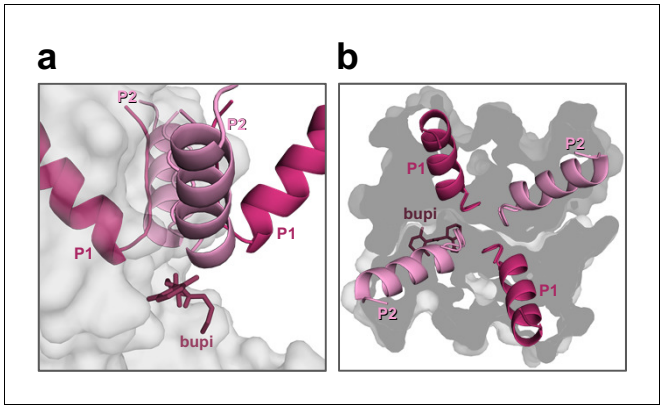

Figure 3—figure supplement 1. Positioning of bupivacaine in the side fenestrations underneath the second pore helices. (**a**) Side-view on a TASK-1 homology model (based on TWIK-1) illustrating the positioning of bupivacaine in the side fenestrations underneath the second pore helices and (**b**) the respective view from the top. Note that only the second pore loops are located above the fenestrations.

DOI: https://doi.org/10.7554/eLife.39476.009

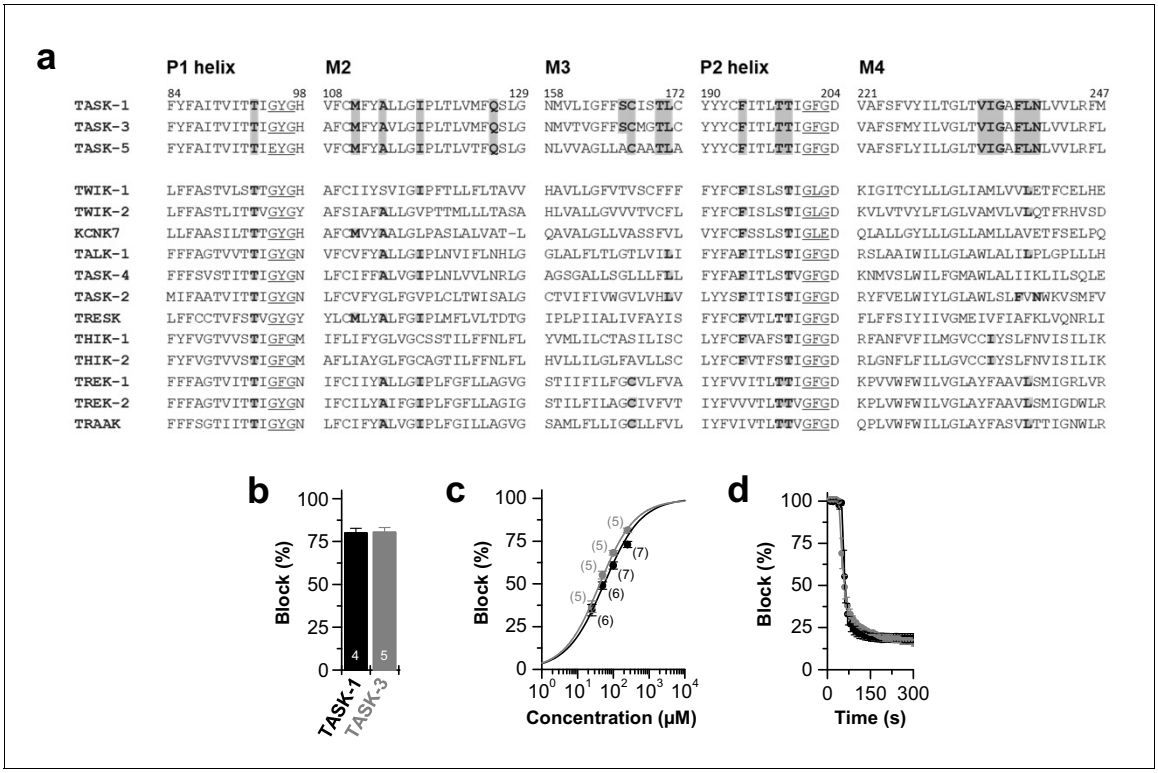

Figure 3—figure supplement 2. Conserved binding site and block of TASK-1 and TASK-3 channels by bupivacaine. (**a**) Partial amino acid alignment illustrating the conserved bupivacaine-binding site in TASK-1 and TASK-3. Residues of the bupivacaine-binding site that were validated after 100 ns MD simulations are highlighted in gray, including residues of the pore helices the M2, M3 and M4 segments. (**b**) Block of TASK-1 and TASK-3 channels by 500 μM racemic bupivacaine. (**c**) Dose-response curves of racemic bupivacaine for TASK-1 and TASK-3. (**d**) Wash-in and onset of TASK-1 and TASK-3 inhibition by 500 μM bupivacaine (n = 3). Data are presented as mean ± S.E.M.. The numbers of experiments (n) are indicated within the bar graphs.
DOI: https://doi.org/10.7554/eLife.39476.010

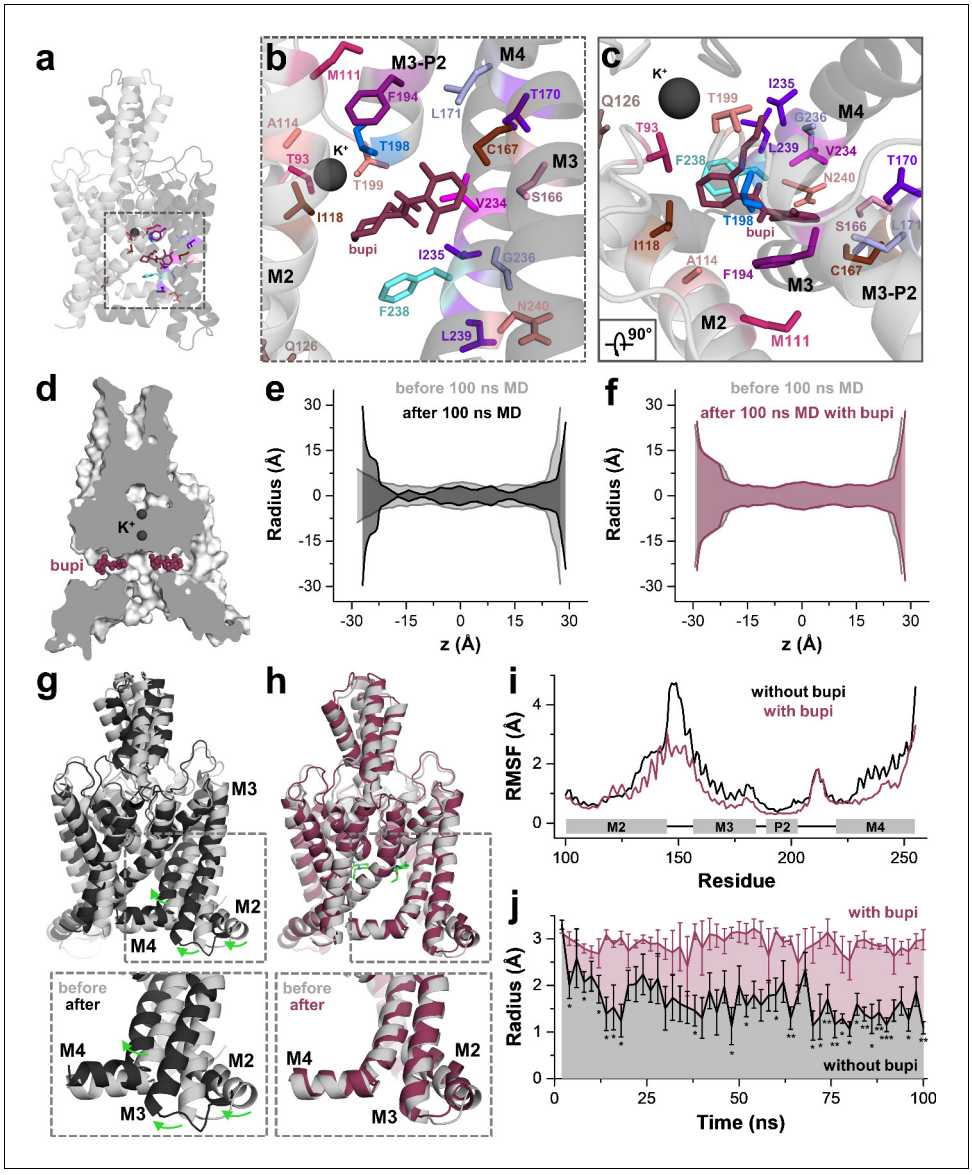

Figure 4. MD simulations - binding in the fenestrations prevents fenestration gating. (**a**) Side view on a TWIK-1 based TASK-1 homology model with bupivacaine located in the side fenestrations after 100 ns MD simulations. (**b–c**) Zoom-ins illustrating 'hit' residues of the alanine scan, which were confirmed in the MD simulations to have contacts with bupivacaine. (**d**) TASK-1 homology model based on TWIK-1 depicting bupivacaine within the two side fenestrations. (**e**) Hole analysis before (light gray) and after (gray) 100 ns MD simulations revealing a collapse of the side fenestrations when the channels move to the 'up' state. (**f**) Hole analysis as in (**e**), but in the presence of bupivacaine (purple), which prevents the movement to the 'up' state and the concomitant collapse of the fenestrations. (**g**) TASK-1 homology model in the absence of bupivacaine before (gray) and after 100 ns of MD simulations (black). Green arrows indicate the movement of the M2, M3 and M4 segments causing the 'down' to 'up' transition. (**h**) TASK-1 homology model in the presence of bupivacaine (green) before (gray) and after (purple) 100 ns, illustrating the lack of the M2, M3 and M4 movements. (**i**) Root-mean-square fluctuations (RMSF) calculated for the alpha carbons of the M2, M3, P2 and M4 segments in the absence and presence of bupivacaine. (**j**) Quantitative analysis of the bottleneck radius of the side fenestrations over the time course of 100 ns MD simulations (n = 4) in the absence (gray) and presence (purple) of bupivacaine. Data are represented as mean ± S.E.M.

DOI: https://doi.org/10.7554/eLife.39476.011

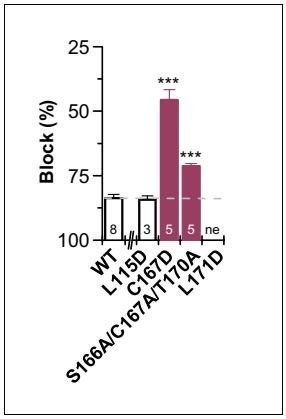

Figure 4—figure supplement 1. Reduced bupivacaine inhibition by M3 mutants. Block by 500 µM bupivacaine, analyzed for additional mutants of the M3 segment that were generated since the MD simulations predicted contacts with those residues. Inhibition was analyzed at +40 mV. Data are presented as mean ± S.E.M.. The numbers of experiments (n) are indicated within the bar graph.

DOI: https://doi.org/10.7554/eLife.39476.012

a

template homology model	acquired poses	successful dockings (%)
TWIK-1 (OO)	40/40	100
TREK-2 (OO)	37/40	92.5
TRAAK (CO)	16/20	80.0
TRAAK (OO)	31/40	77.5

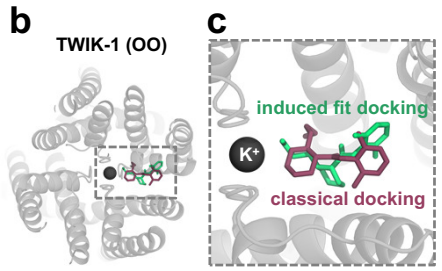

Figure 4—figure supplement 2. Induced fit docking experiments predict a bupivacaine binding mode highly similar to that of classical docking experiments. (**a**) For each of the four different homology models a total of 20 structures (seeds) were generated by MDs taking a frame every 0.5 ns. Induced fit dockings were performed at the 20 structures per model with 40 or 20 open fenestrations if only one fenestration is in the open state. Only in the TASK-1 model based on TWIK-1 (OO), induced fit dockings identified poses for each structure and for each fenestration (40/40; 100%). (**b**) Top view of the docking solution in a TWIK-1 (OO) based TASK-1 homology model with the lowest induced fit docking energy, while being compatible with the TEA versus TPA competition experiments. (**c**) Zoom-in of the top view from (**b**): induced fit dockings predict a binding model (green) similar to that proposed by classical docking experiments and MD simulations (purple) (***Figure 4a–c***).
DOI: https://doi.org/10.7554/eLife.39476.013

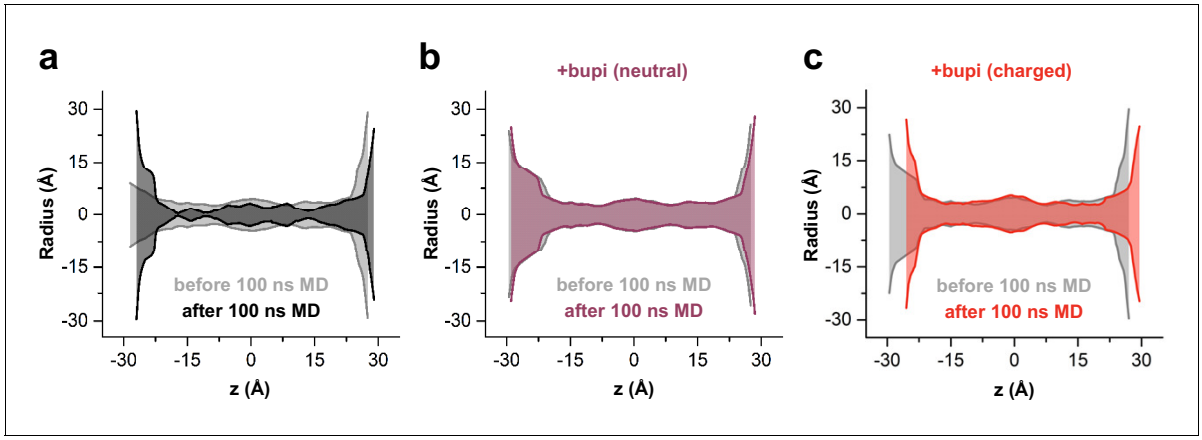

Figure 4—figure supplement 3. MD simulations - binding in the fenestrations prevents fenestration gating. (**a**) Hole analysis of TWIK-1 based TASK-1 homology model before (light gray) and after (gray) 100 ns MD simulation, revealing a collapse of the side fenestrations when the channels move to the 'up' state. (**b**) Hole analysis as in (**a**), but in the presence of neutral or (**c**) charged bupivacaine, which prevents the movement to the 'up' state and the concomitant collapse of the fenestrations.

DOI: https://doi.org/10.7554/eLife.39476.014

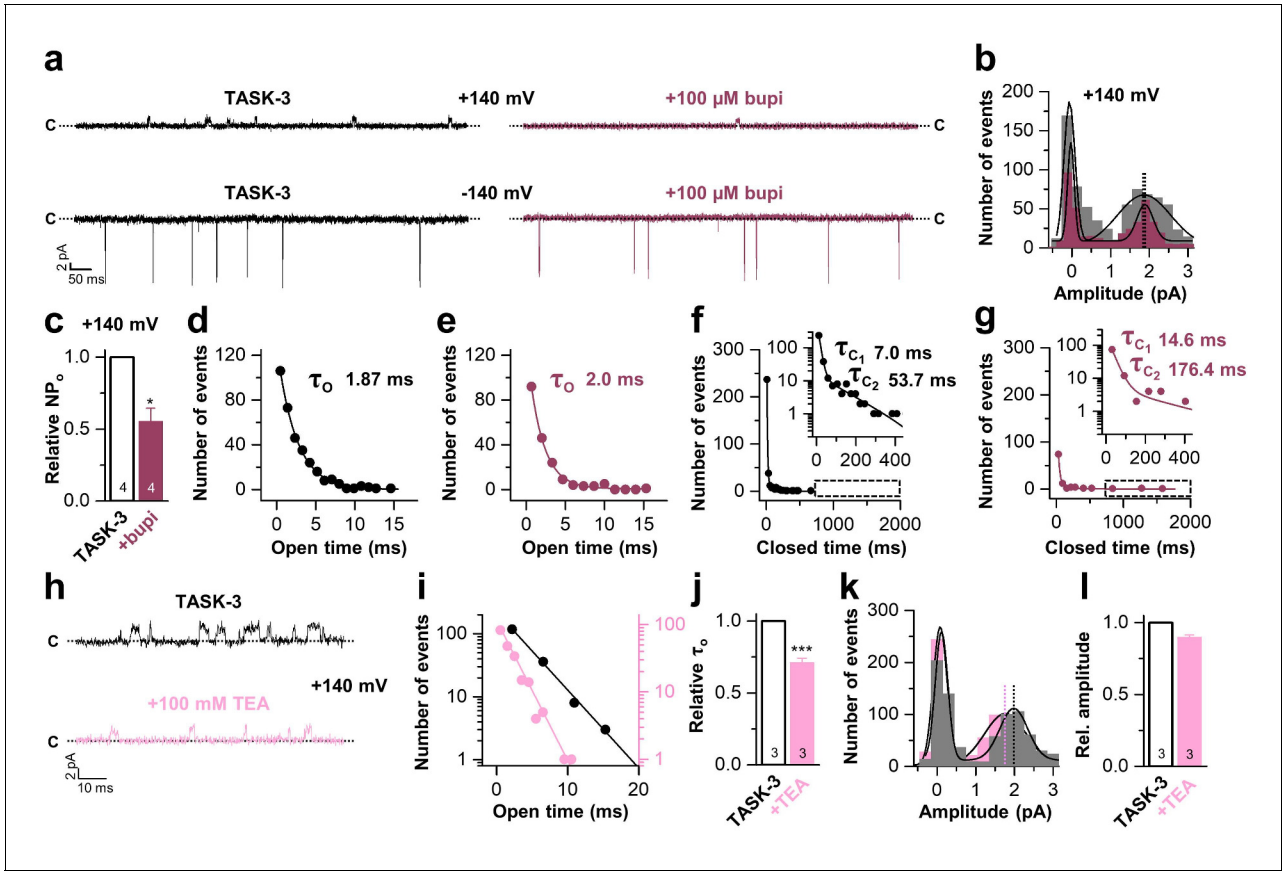

Figure 5. Bupivacaine stabilizes the closed state of TASK channels. (**a**) Representative inside-out single channel recordings of TASK-3 at +140 and −140 mV before (left, black) and after (right, purple) application of 100 µM bupivacaine and (**b**) amplitude histogram of the events recorded at +140 mV (n = 4). (**c**) Change in relative open probability (NP_o) by 100 µM bupivacaine. (**d**) Graphical illustration of the open times before and (**e**) after drug application (n = 4). (**f**) Analyses of the closed time before and (**g**) after application of 100 µM bupivacaine (n = 4). (**h**) Representative inside-out single channel recordings of TASK-3 at +140 mV before (up, black) and after (down, light pink) application of 100 mM TEA and (**i**) representative illustration of the open times of a TASK-3 containing patch before and after drug application. (**j**) Relative change in open times by 100 mM TEA (n = 3). (**k**) Amplitude histogram of the events recorded at +140 mV (n = 3) and (**l**) the respective analyses of the relative change in single channel amplitude before (black) and after (light pink) application of 100 mM TEA. Data are represented as mean ± S.E.M.. The numbers of experiments (n) are indicated within the respective bars.

DOI: https://doi.org/10.7554/eLife.39476.016

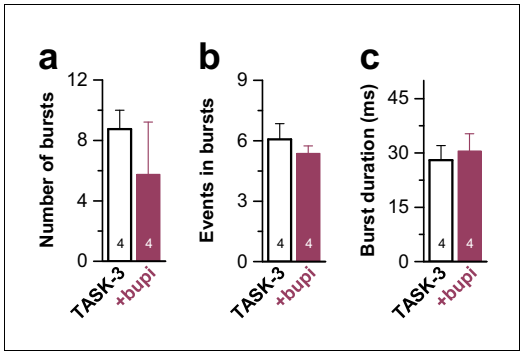

Figure 5—figure supplement 1. Analyses of the single channel burst characteristics of TASK-3 after application of bupivacaine. TASK-3 single channel burst kinetics analyzed after application of 100 µM bupivacaine to the cytosolic phase of inside-out patches. Data are presented as mean ± S.E.M.. The numbers of experiments (n) are indicated within the bar graphs.

DOI: https://doi.org/10.7554/eLife.39476.017

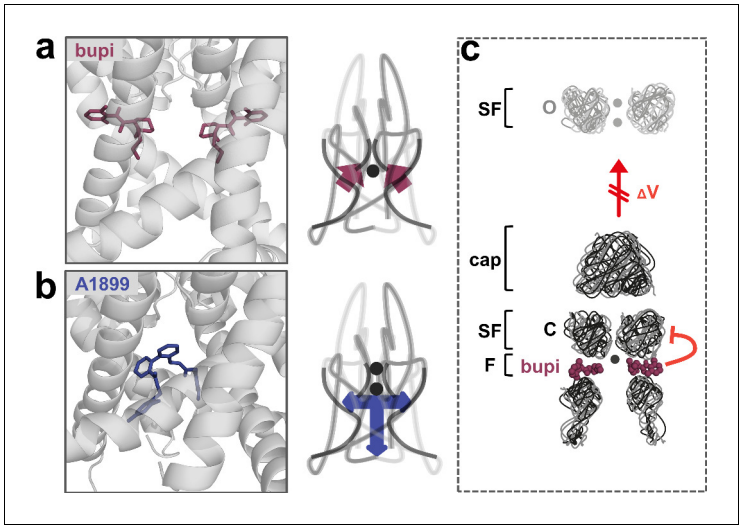

Figure 6. A novel allosteric inhibition mechanism interferes with the voltage-dependent activation of TASK channels. (**a**) Illustration of the bupivacaine binding mode in the side fenestrations (left), preventing K^+-flux gating, which requires a K^+ filled selectivity filter (right cartoon). The closed state or collapsed selectivity filter is indicated by one potassium ion (black dot). (**b**) A1899 located in the central cavity (left) is binding in an 'anchor'-shaped like structure which occludes the pore and thus prevents K^+ permeation (right cartoon). Here the K^+ occupancy of the selectivity filter is not disturbed (illustrated by two black dots in the selectivity filter). (**c**) Schematic illustration of the proposed gating model of TASK-1. The upper panel illustrates the selectivity filter in the open state and the lower panel the TASK channel. 'C' indicates the closed state conformation of the selectivity filter (one potassium ion located before the collapsed filter) and 'O' indicates the open state with a K^+ filled selectivity filter (here two potassium ions illustrated). SF indicates the selectivity filter and F the side fenestrations. The voltage-dependent (ΔV) opening of the selectivity filter gate (K^+-flux gating) preferentially results in the typical outwardly rectifying K^+ currents. The presence of bupivacaine in the side fenestrations prevents the voltage-dependent K^+-flux gating, resulting in reduced outward currents at depolarized potentials and thus a voltage-dependent inhibition.
DOI: https://doi.org/10.7554/eLife.39476.018